Supplemental Information for

Temporal Multilevel Luminescence Anti-Counterfeiting through Scattering Media

Meiling Tan[1,2,3], Feng Li[1,2,3], Xing Wang[4], Rongwei Fan[4], and Guanying Chen[1,2,3]*

[1]MIIT Key Laboratory of Critical Materials Technology for New Energy Conversion and Storage, School of Chemistry and Chemical Engineering, Harbin Institute of Technology, 150001 Harbin, People's Republic of China.

[2]Key Laboratory of Micro-systems and Micro-structures, Ministry of Education, Harbin Institute of Technology, 150001 Harbin, People's Republic of China.

[3]State Key Laboratory of Urban Water Resource and Environment, School of Chemistry and Chemical Engineering, Harbin Institute of Technology, Harbin 150001, People's Republic of China.

[4]National Key Laboratory of Tunable Lasers, Institute of Optical-Electronics, Harbin Institute of Technology, 150001 Harbin, People's Republic of China.

*Correspondence: chenguanying@hit.edu.cn

TABLE OF CONTENTS

Fig. S14. Time-delayed SWIR luminescence imaging through 6 mm intralipid layer.

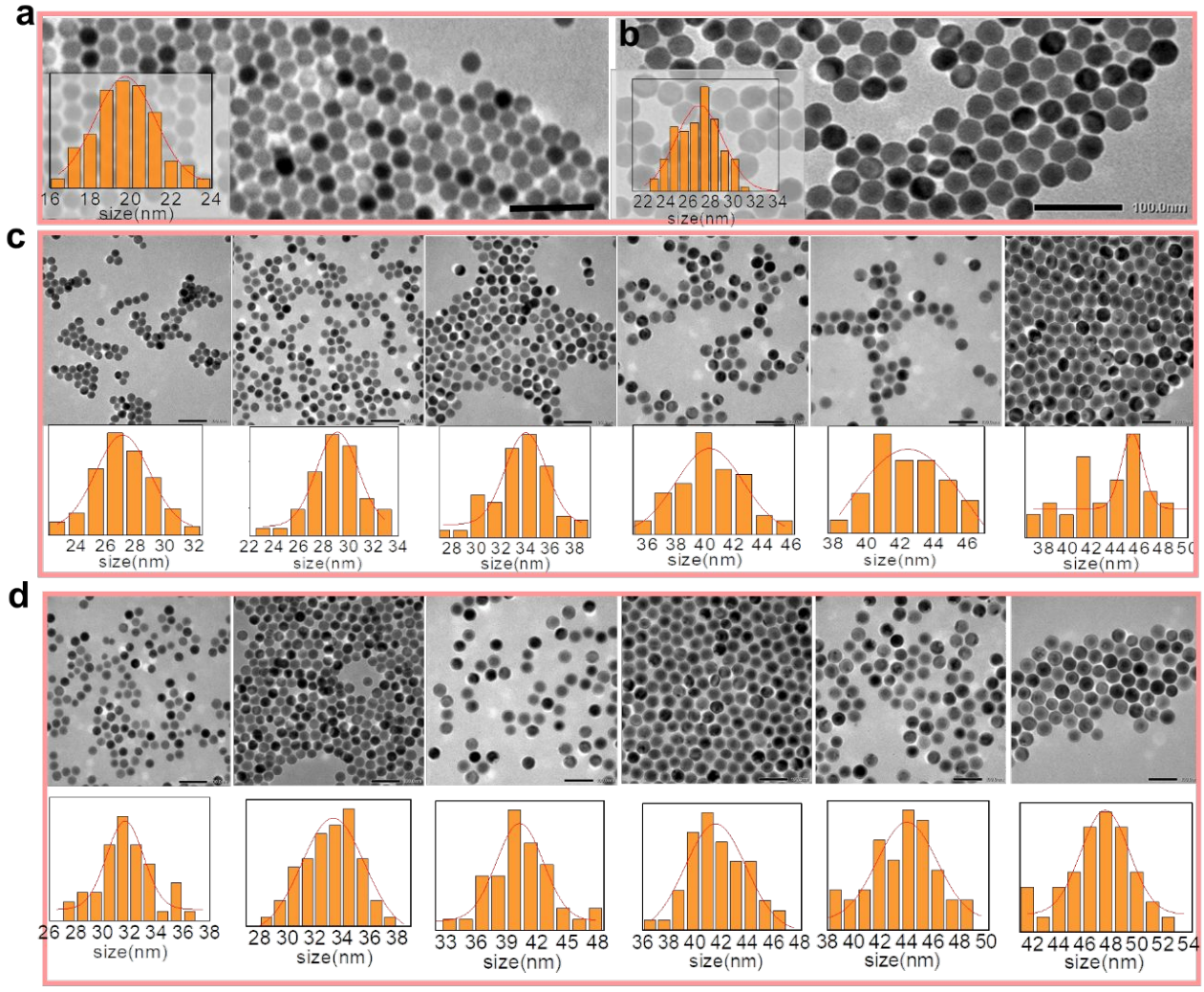

Figure S1. Transmission electron microscopy **(**TEM) images of (a) the core $NaYF_4$: 20% Yb^{3+}, 40% Er^{3+}, (b) the core/shell $NaYF_4$: 20% Yb^{3+}, 40% Er^{3+}@ $NaYbF_4$, (c) the core/shell/shell $NaYF_4$: 20% Yb^{3+}, 40% Er^{3+}@ $NaYbF_4$@ $NaYF_4$ NPs with varying thickness, and (d) the core/shell/shell/shell $NaYF_4$: 20% Yb^{3+}, 40% Er^{3+}@ $NaYbF_4$@ $NaYF_4$@ $NaYF_4$:20% Nd^{3+} nanoparticles. The insets in (a) and (b) show the corresponding size distributions of nanoparticles in (a) and (b), while the corresponding size distributions for nanoparticles in (c) and (d) are displayed right below the TEM images. The size of the core $NaYF_4$: 20% Yb^{3+}, 40% Er^{3+} nanoparticles was measured to be about 19.7 nm, while the thickness of the $NaYbF_4$ layer was estimated to be about 3.2 nm by comparing the size difference between the core/shell and the parent core nanoparticles. The size increase from the core/shell in (b) to the core/shell/shell nanoparticles in (c) suggests that the thickness of $NaYF_4$ shell layer varies from ~ 1.04, 1.94, 2.45, 6.73, 7.70, to ~ 8.55 nm. In addition, the size difference between nanoparticles in (c) and (d) implies that the outmost shell layer has an almost identical thickness of ~ 2 nm for all the resultant core/multi-shell nanoparticles.

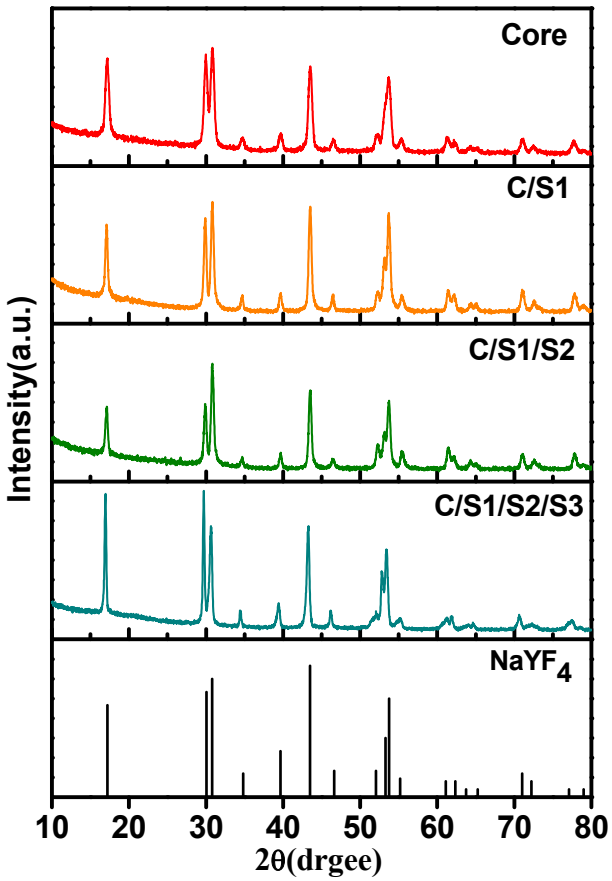

Figure S2. X-ray diffraction (XRD) patterns of the core $NaYF_4$: 20% Yb^{3+}, 40% Er^{3+} (marked as core), the core/shell $NaYF_4$: 20% Yb^{3+}, 40% Er^{3+}@ $NaYbF_4$ (marked as C/S1), the core/shell/shell $NaYF_4$: 20% Yb^{3+}, 40% Er^{3+}@$NaYbF_4$@$NaYF_4$ NPs with a $NaYF_4$ layer of 7.70 nm (marked as C/S1/S2), and the core/shell/shell/shell $NaYF_4$: 20% Yb^{3+}, 40% Er^{3+}@ $NaYbF_4$@ $NaYF_4$@ $NaYF_4$:20% Nd^{3+} nanoparticles (marked as C/S1/S2/S3). The standard diffraction pattern of hexagonal crystal phase $NaYF_4$ (JCPDS No. 16-0334) is also included for reference.

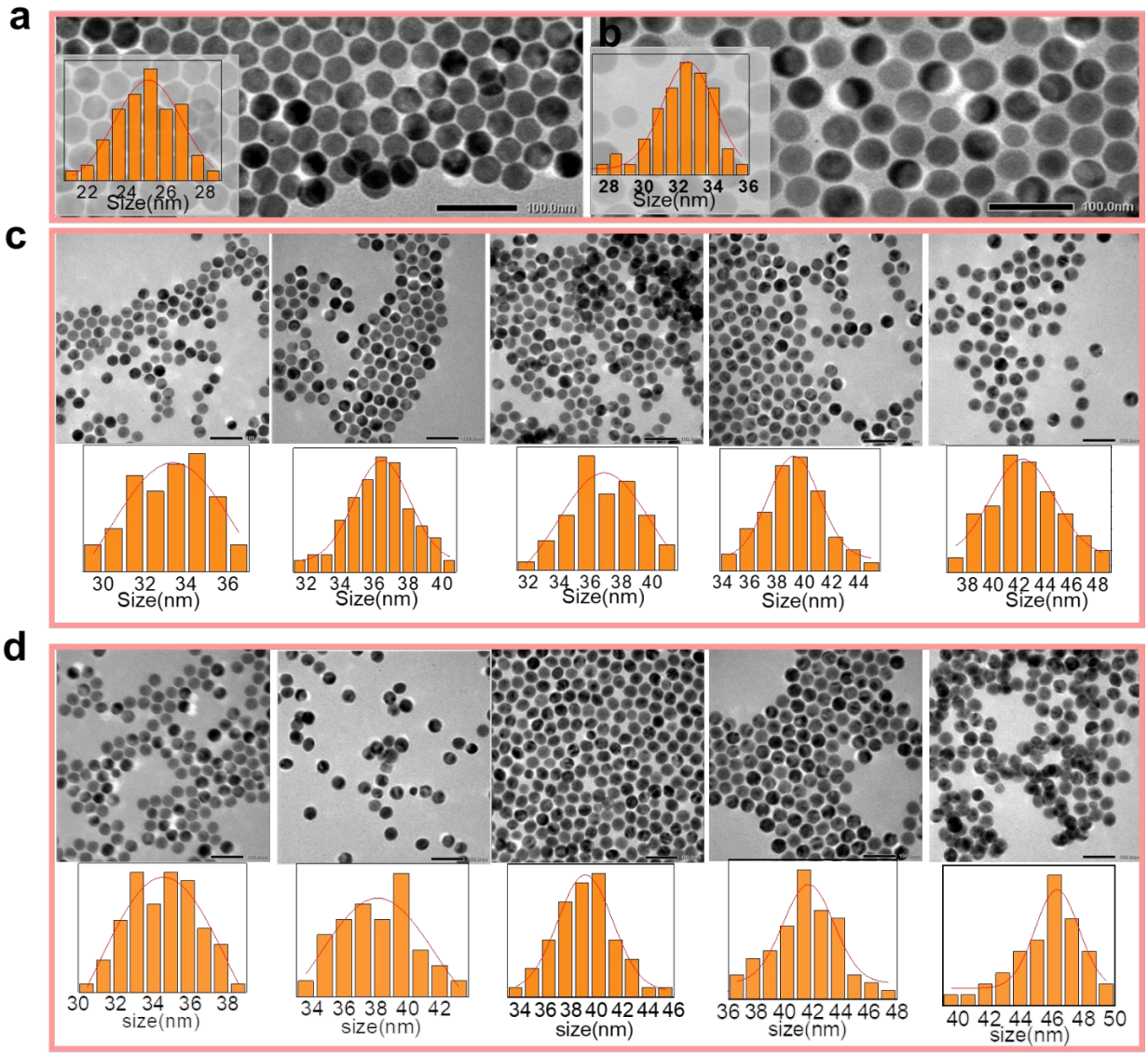

Figure S3. TEM images and size distributions of (a) the core $NaYF_4$: 20% Yb^{3+}, 2% Er^{3+}, (b) the core/shell $NaYF_4$: 20% Yb^{3+}, 2% Er^{3+} @$NaYbF_4$, (c) the core/shell/shell $NaYF_4$: 20% Yb^{3+}, 2% Er^{3+}@ $NaYbF_4$@ $NaYF_4$ NPs with varying thickness, and (d) the core/shell/shell/shell $NaYF_4$: 20% Yb^{3+}, 2% Er^{3+}@ $NaYbF_4$@ $NaYF_4$@ $NaYF_4$:20% Nd^{3+} nanoparticles. The insets in (a) and (b) show the corresponding size distributions of nanoparticles in (a) and (b), while the corresponding size distributions for nanoparticles in (c) and (d) are displayed right below the TEM images. The size of the core $NaYF_4$: 20% Yb^{3+}, 2% Er^{3+} nanoparticles was measured to be about 25 nm, while the thickness of the $NaYbF_4$ layer was estimated to be about 3.5 nm. A comparison of the size difference between (b) and (c) suggests that the thickness of $NaYF_4$ shell layer varies from ~ 1.01, 2.02, 2.79, 3.46, to 5.07 nm. In addition, the size difference between nanoparticles in (c) and (d) implies that the outmost shell layer has an almost identical thickness of ~ 1-2 nm for all the resultant core/multi-shell nanoparticles.

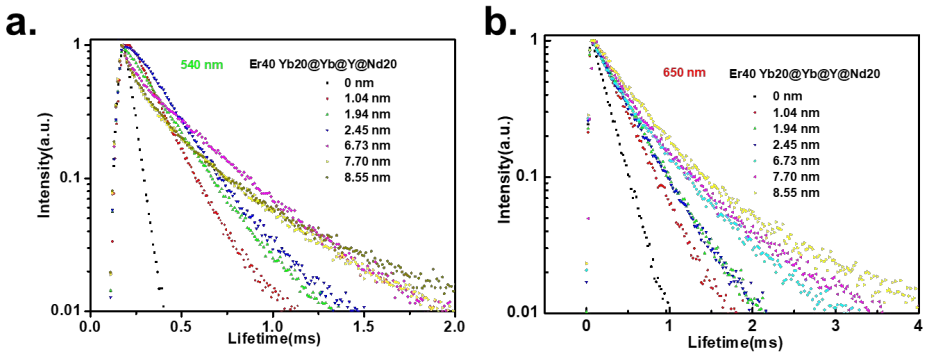

Figure S4.Upconversion luminescence decay curves at (a) 540 nm and (b) 650 nm of $NaYF_4$: 20% Yb^{3+}, 40% Er^{3+} @ $NaYbF_4$@ $NaYF_4$@ $NaYF_4$:20% Nd^{3+} nanoparticles with varying $NaYF_4$ thickness, measured under 808 nm pulsed laser excitation. Both decay curves at 540 and 650 nm were gradually extended with an increase of the $NaYF_4$ shell thickness.

As one can see, the rise times for samples with 0 nm to 2.45 nm are similar and longer than the samples with 6.73 nm to 8.55 nm. Moreover, the upconverted luminescence decay curves at 540 nm can be fitted by a single-exponential for samples with 0 nm to 2.45 nm, while by double-exponential for samples with 6.73 nm to 8.55 nm, thus resulting in observation of cross-overs.

These observations, we believe, arise from two distinct pathways to produce green-emitting upconversion luminescence at 540 nm. (i) The designated pathway of $Nd^{3+} \rightarrow Yb^{3+} \rightarrow Er^{3+}$ from the outer layer to the core region, which can be regulated by the thickness of the energy-retarding $NaYF_4$ layer. (ii) Direct excitation of Er^{3+} ions by the 800 nm excitation light, resulting in green-emitting upconversion through excited state absorption (ESA) or energy transfer upconversion (ETU) mechanisms. This route is independent of the energy-retarding $NaYF_4$ layer, possessing a faster start-up. The first route dominates over the second one for the thickness of 0 nm to 2.45 nm, while the second route becomes competitive to the first one for the thickness of 6.73 nm to 8.55 nm, as the upconversion luminescence decline substantially at larger thicknesses, particular for the 6.73-8.55 nm. We believe this reason causes thickness-dependent single- and double- exponential upconversion decay behaviors and thus cross-overs. Indeed, when fitting data with bi-exponential for samples with thicker $NaYF_4$ (6.73-8.55 nm), longer luminescence decays at thicker shell thicknesses can also be observed (Table S1).

Table S1. The fitted values of lifetime at 540 nm of $NaYF_4$: 20% Yb^{3+}, 40% Er^{3+}@ $NaYbF_4$@ $NaYF_4$@ $NaYF_4$:20% Nd^{3+} nanoparticles

Nanoparticles with different shell thickness of $NaYF_4$ layer(nm)	Fitted values of lifetime at 540 nm(μs)
0	τ=54.1
1.04	τ=159.9
1.94	τ=188.3
2.45	τ=212.6
6.73	τ_1=287.0; τ_2=36.6
7.70	τ_1=320.0; τ_2=55.7
8.55	τ_1=356.2; τ_2=70.7

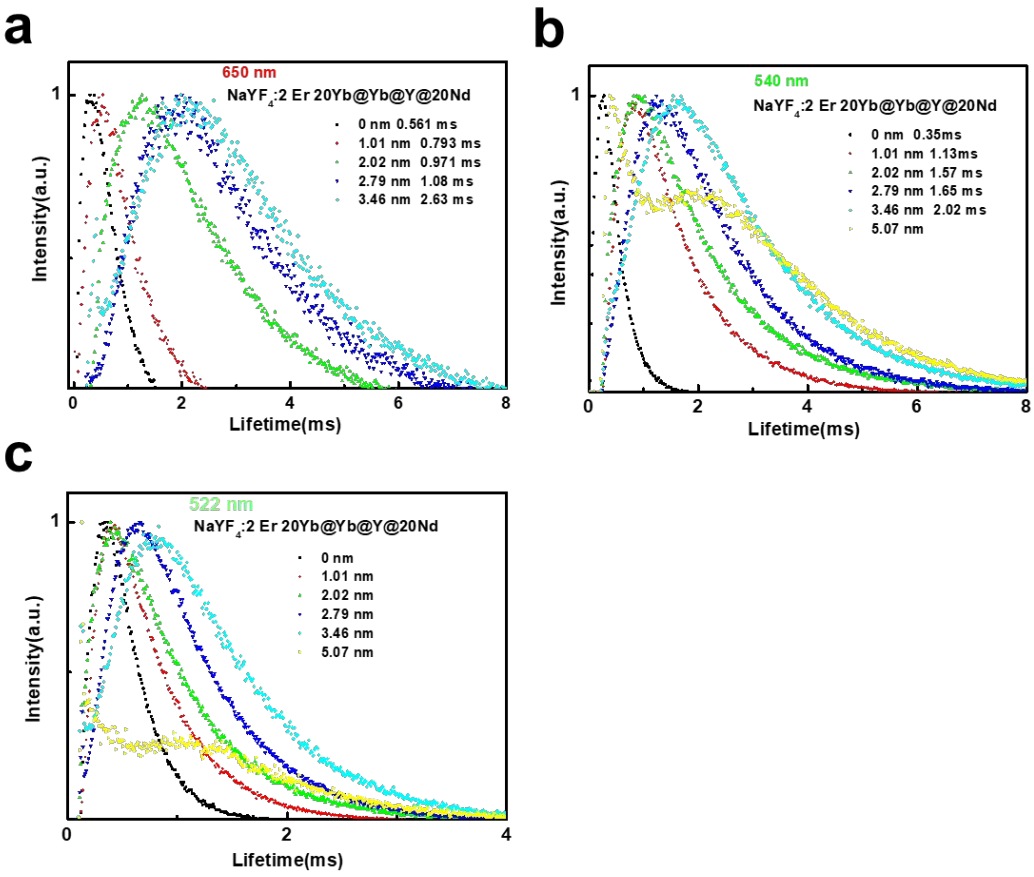

Figure S5. Upconversion luminescence decay curves at (a) 650 nm, (b) 540 nm and (c) 522 nm of $NaYF_4$: 20% Yb^{3+}, 2% Er^{3+}@ $NaYbF_4$@ $NaYF_4$@ $NaYF_4$:20% Nd^{3+} NPs with varying $NaYF_4$ thickness, measured under pulsed laser excitation at 808 nm. All the decay curves at 650 nm, 540 nm and 522 nm are gradually extended with an increase of the $NaYF_4$ shell thickness.

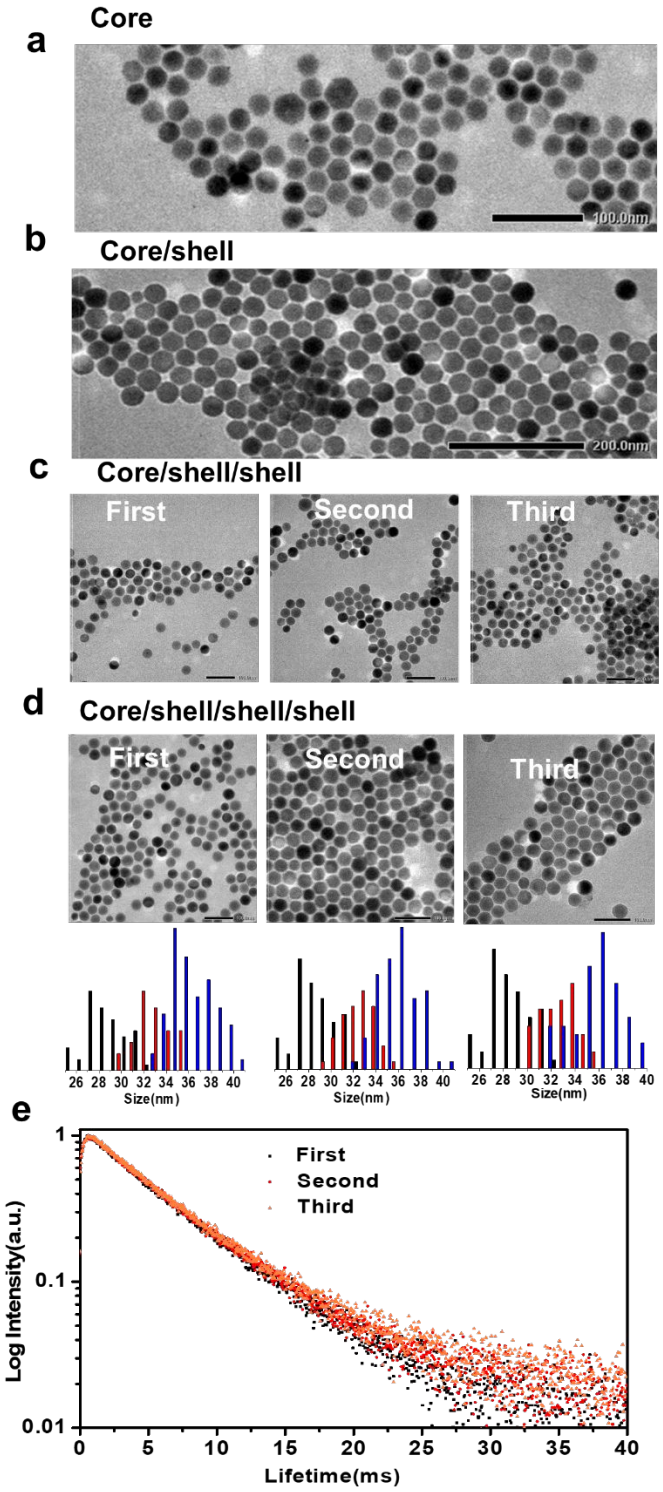

Figure S6. TEM images of (a) the core $NaYF_4$: 20% Yb^{3+}, 40% Er^{3+}, (b) the core/shell $NaYF_4$: 20% Yb^{3+}, 40% Er^{3+}@ $NaYbF_4$, (c) the core/shell/shell $NaYF_4$: 20% Yb^{3+}, 40% Er^{3+}@ $NaYbF_4$@ $NaYF_4$ nanoparticles prepared in three different batches, (d) the core/ shell/ shell /shell $NaYF_4$: 20% Yb^{3+}, 40% Er^{3+}@ $NaYbF_4$@ $NaYF_4$@ $NaYF_4$:20% Nd^{3+} nanoparticles prepared in three different batches. (d) The size distribution histograms for the core/shell (black), the core/shell/shell (red), and the core/shell/shell/shell (blue) nanoparticles prepared in three different batches. (e) Measured luminescence decay curves at 1532 nm from the resultant core/ shell/ shell /shell nanoparticles prepared in three different batches.

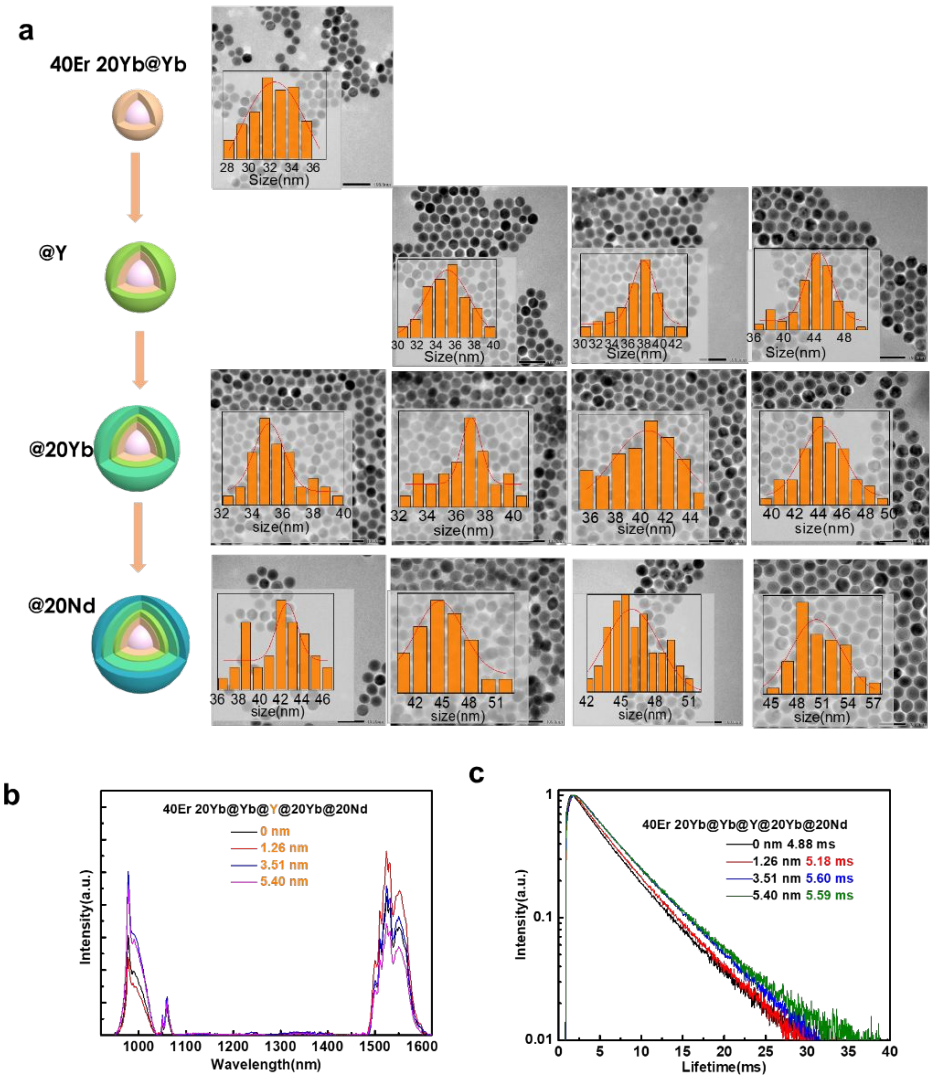

Figure S7. TEM and spectral results for the core/multi-shell $NaYF_4$: 20% Yb^{3+}, 40% Er^{3+}@ $NaYbF_4$@ $NaYF_4$@ $NaYF_4$:20% Yb^{3+}@ $NaYF_4$:20% Nd^{3+} nanoparticles with the inert shell $NaYF_4$ placed between the $NaYbF_4$ shell layer and the $NaYF_4$: 20% Yb^{3+} shell layer. (a) TEM images of the parent core/shell $NaYF_4$: 20% Yb^{3+}, 40% Er^{3+}@ $NaYbF_4$ nanoparticles, the core/shell/shell $NaYF_4$: 20% Yb^{3+}, 40% Er^{3+}@ $NaYbF_4$@ $NaYF_4$ nanoparticles with varied $NaYF_4$ shell layer thickness, the core/shell/shell/shell $NaYF_4$: 20% Yb^{3+}, 40% Er^{3+}@ $NaYbF_4$@ $NaYF_4$@ $NaYF_4$:20% Yb^{3+} nanoparticles, and the core/shell/shell/ shell/shell $NaYF_4$: 20% Yb^{3+}, 40% Er^{3+}@ $NaYbF_4$@ $NaYF_4$@ $NaYF_4$:20% Yb^{3+}@ $NaYF_4$:20% Nd^{3+} nanoparticles. The energy-retarding $NaYF_4$ shell layer thickness was varied from 0, 1.26, 3.51, to 5.40 nm. (b) Shortwave infrared (SWIR) luminescence spectra of all the core/multi-shell $NaYF_4$: 20% Yb^{3+}, 40% Er^{3+}@ $NaYbF_4$@ $NaYF_4$@ $NaYF_4$:20% Yb^{3+}@ $NaYF_4$:20% Nd^{3+} nanoparticles with varied thickness of $NaYF_4$ shell under 808 nm excitation. All core/multi-shell nanoparticles present intense SWIR luminescence as that of the counterpart one without energy-retarding layer. (c) Luminescence decay curves measured at 1532 nm for the core/multi-shell $NaYF_4$: 20% Yb^{3+}, 40% Er^{3+}@ $NaYbF_4$@ $NaYF_4$@ $NaYF_4$:20% Yb^{3+}@ $NaYF_4$:20% Nd^{3+} nanoparticles with varied thickness of $NaYF_4$. The decay curves are gradually extended with an increase of the $NaYF_4$ layer shell thickness, substantiating the importance of energy retarding processes for luminescence lifetime control.

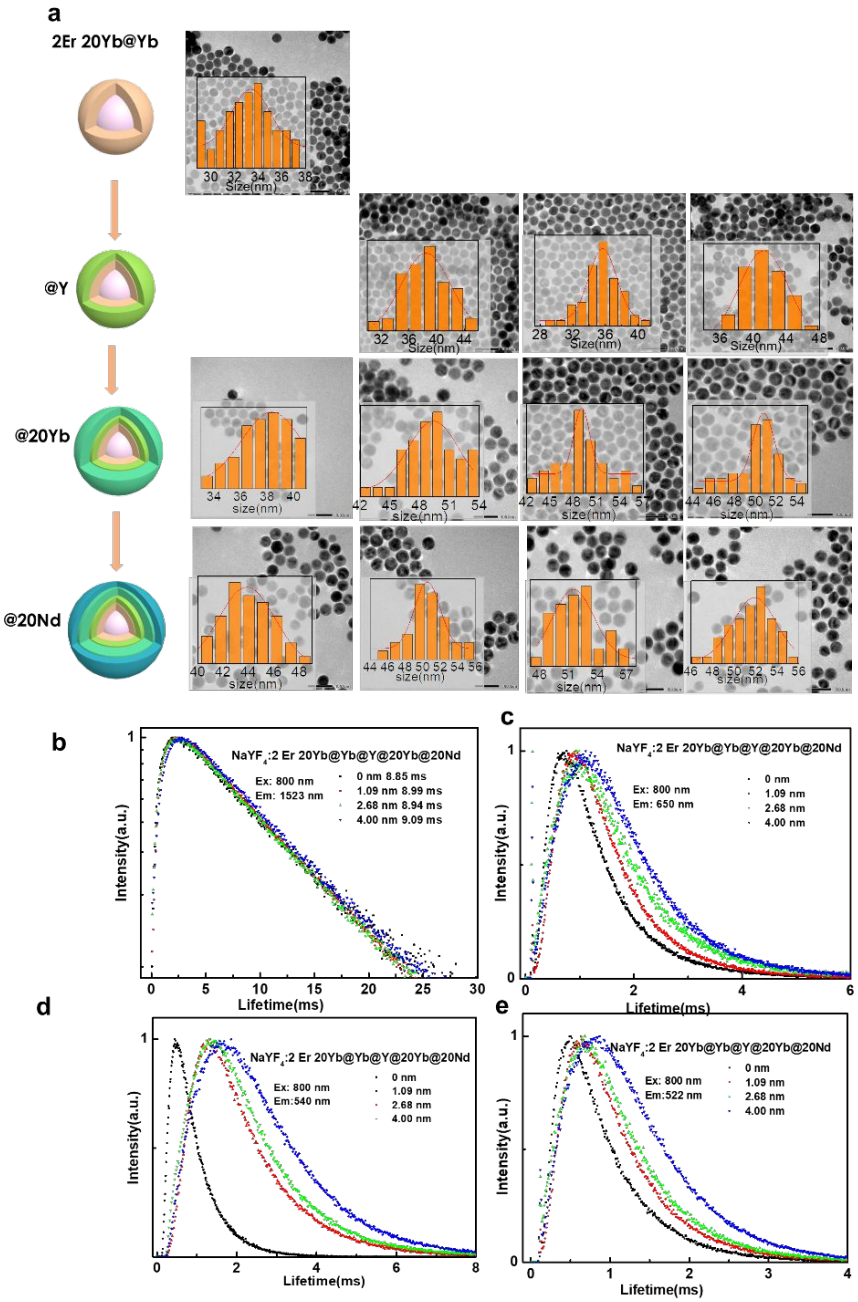

Figure S8. (a) TEM images of the parent core/shell $NaYF_4$: 20% Yb^{3+}, 2% Er^{3+}@ $NaYbF_4$ nanoparticles, the core/shell/shell $NaYF_4$: 20% Yb^{3+}, 2% Er^{3+}@ $NaYbF_4$@ $NaYF_4$ nanoparticles with varied $NaYF_4$ shell layer thickness, the core/shell/shell/shell $NaYF_4$: 20% Yb^{3+}, 2% Er^{3+}@ $NaYbF_4$@ $NaYF_4$@ $NaYF_4$:20% Yb^{3+} nanoparticles, and the core/shell/shell/shell/shell $NaYF_4$: 20% Yb^{3+}, 2% Er^{3+}@ $NaYbF_4$@ $NaYF_4$@ $NaYF_4$:20% Yb^{3+}@ $NaYF_4$:20% Nd^{3+} nanoparticles. The energy-retarding $NaYF_4$ shell layer thickness was varied from 0, 1.09, 2.44, to 4.00 nm. Measured decay curves of down-shifting luminescence at (b) 1532 nm, and upconversion luminescence at (c) 650 nm, (d) 540 nm, and (e) 522 nm for the core/multi-shell $NaYF_4$: 20% Yb^{3+}, 2% Er^{3+}@ $NaYbF_4$@ $NaYF_4$@ $NaYF_4$:20% Yb^{3+}@ $NaYF_4$:20% Nd^{3+} nanoparticles with varied thickness of $NaYF_4$ shell layer under pulsed laser excitation at 808 nm. All decay curves for both down-shifting and upconversion luminescence are gradually prolonged with an increase of the shell thickness of $NaYF_4$ layer, demonstrating the important role of the energy-retarding $NaYF_4$ layer for luminescence lifetime control.

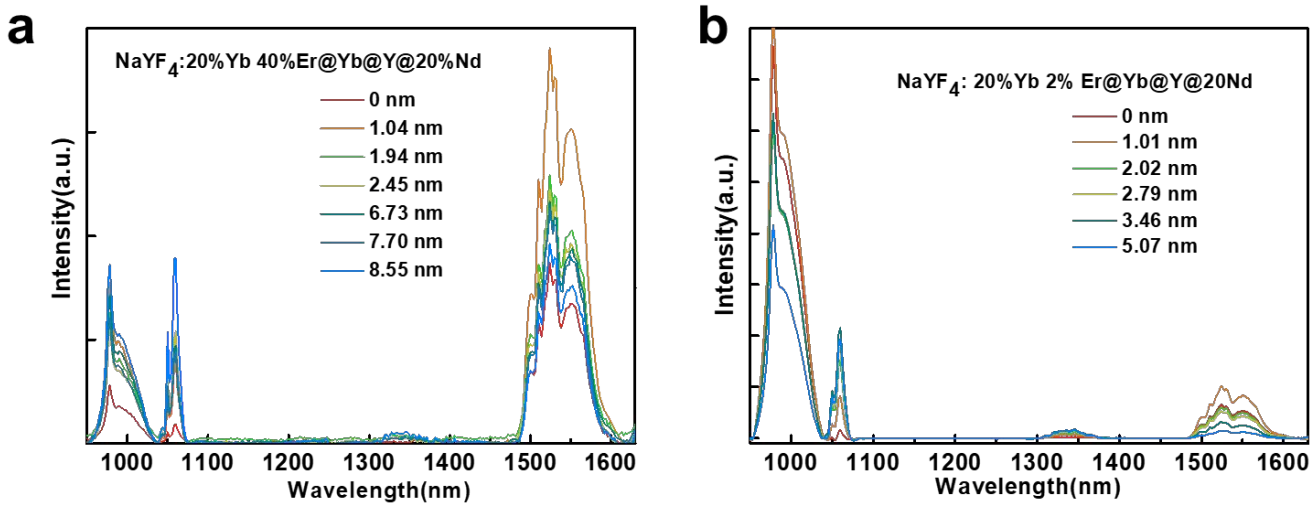

Figure S9. SWIR luminescence spectra of (a) $NaYF_4$: 20% Yb^{3+}, 40% Er^{3+}@ $NaYbF_4$@ $NaYF_4$@ $NaYF_4$: 20% Nd^{3+} and (b) $NaYF_4$: 20% Yb^{3+}, 2% Er^{3+}@ $NaYbF_4$@ $NaYF_4$@ $NaYF_4$: 20% Nd^{3+} core/multi-shell nanoparticles with varied $NaYF_4$ shell thickness under 800 nm laser excitation. The high Er^{3+}-containing core/multi-shell nanoparticles in (a) present enhanced luminescence as compared to the core/multi-shell one with null $NaYF_4$ shell thickness, while the low Er^{3+}-containing core/multi-shell nanoparticles in (b) presents intense luminescence on the same level as that of the core/multi-shell nanoparticles without the $NaYF_4$ shell layer.

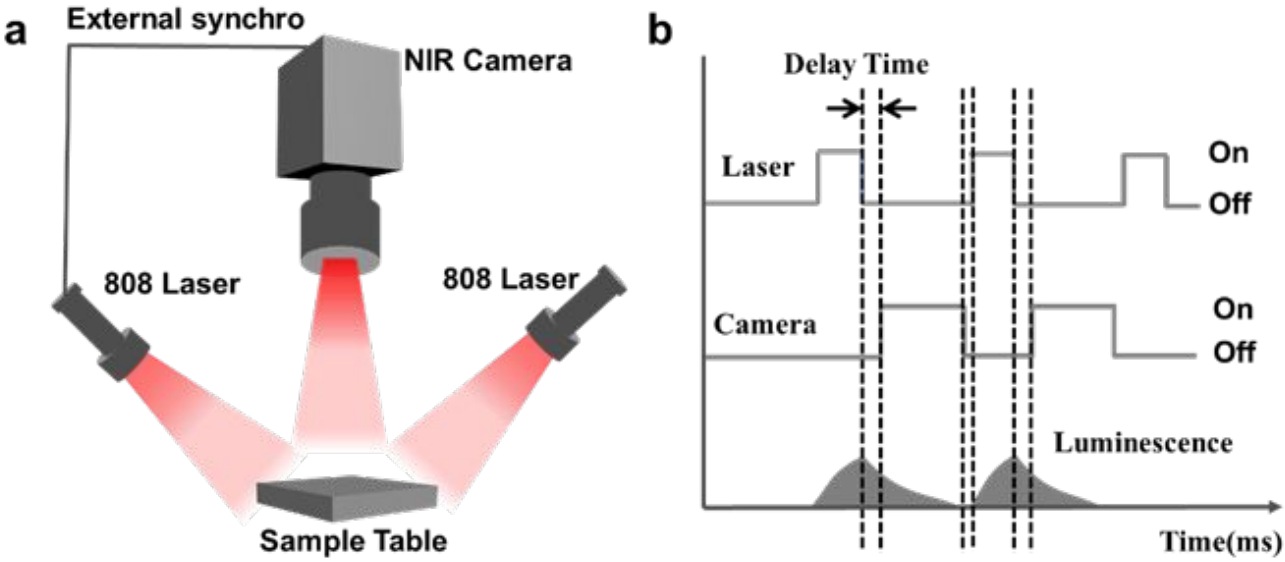

Figure S10. (a) A schematic illustration of our home-built time-resolved SWIR imaging system. (b) A portray of the principle of time-delayed optical imaging, in which the camera is switched on at a defined delay time after the stoppage of the laser signal, and then switched off about ~ 15 μs before next laser pulse.

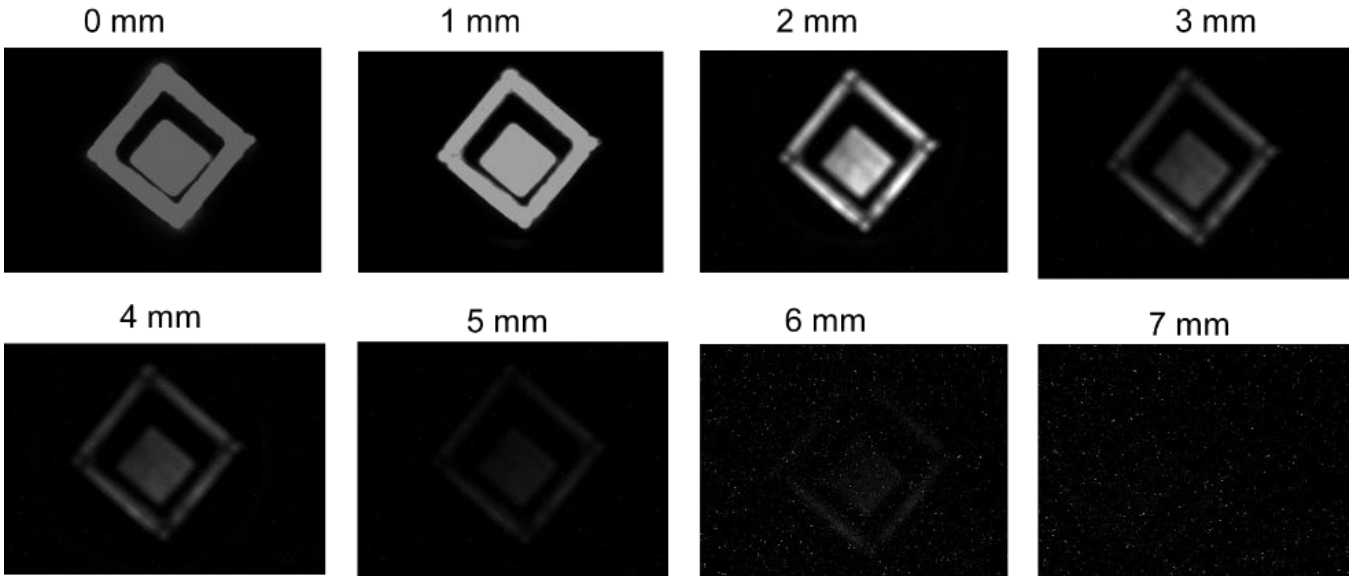

Figure S11. Steady-state SWIR luminescence imaging of a two-square pattern (each square was encoded with $NaYF_4$: 20% Yb^{3+}, 40% Er^{3+}@ $NaYbF_4$@ $NaYF_4$@ $NaYF_4$: 20% Nd^{3+}core/multi-shell nanoparticles of distinct lifetimes; the inner solid square, 6.37 ms; the outer square, 4.03 ms) through biomimetic 1% intralipid layer of varying depth. The luminescence pattern images were collected under 800 nm excitation (120 mW/cm^2) using a 1532 nm band-pass filter. It can be seen that the penetration depth can reach about ~ 6 mm.

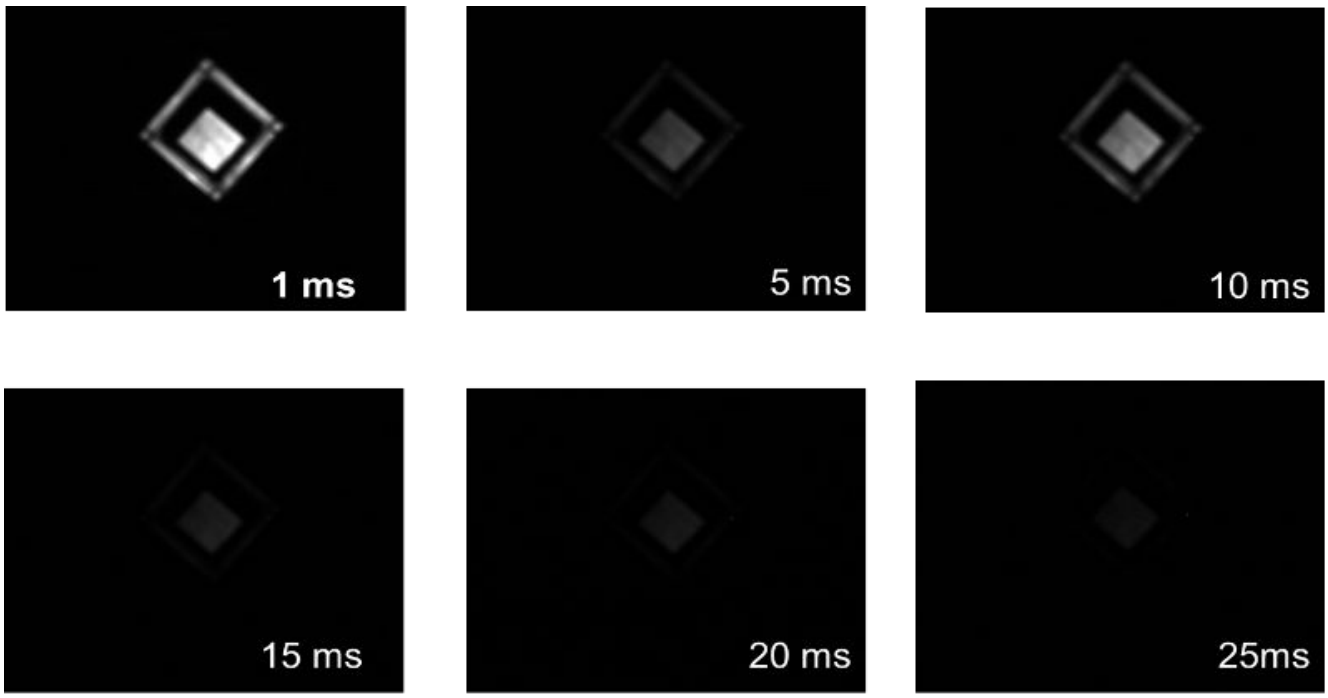

Figure S12. Time-delayed SWIR luminescence imaging of the two-square pattern encoded with $NaYF_4$: 20% Yb^{3+}, 40% Er^{3+}@ $NaYbF_4$@ $NaYF_4$@ $NaYF_4$: 20% Nd^{3+}core/multi-shell nanoparticles of two distinct lifetimes (6.37 and 4.03 ms) through 1 mm intralipid solution, displayed in grayscale. The delay time was varied from 1 to 26 ms. Along with the increase of delay time, the outside boundary square gradually disappeared (4.03 ms), leaving only the inner solid square encoded with longer-lifetime core/multi-shell nanoparticles (6.37 ms).

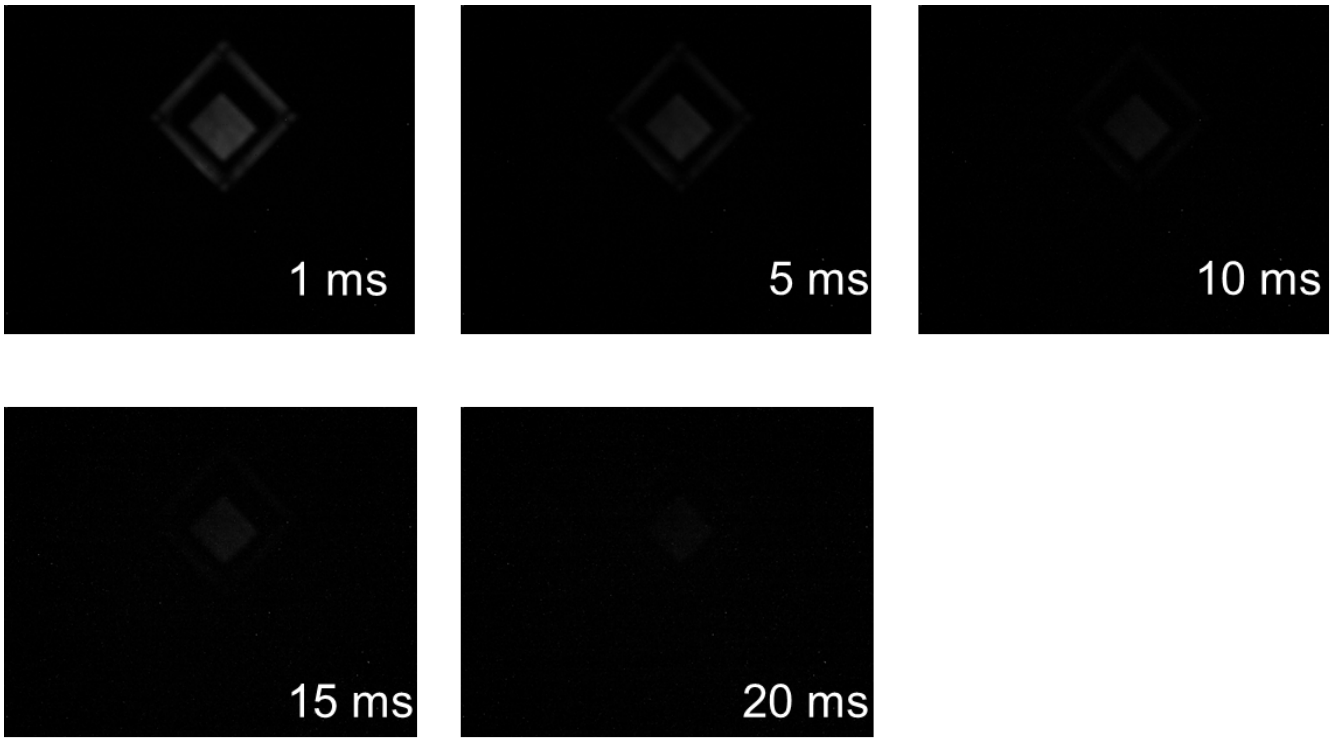

Figure S13. Time-delayed luminescence imaging of the two-square pattern encoded with $NaYF_4$: 20% Yb^{3+}, 40% Er^{3+}@ $NaYbF_4$@ $NaYF_4$@ $NaYF_4$: 20% Nd^{3+}core/multi-shell nanoparticles of two distinct lifetimes (6.37 and 4.03 ms), which was immersed in intralipid solution at a 3 mm depth.

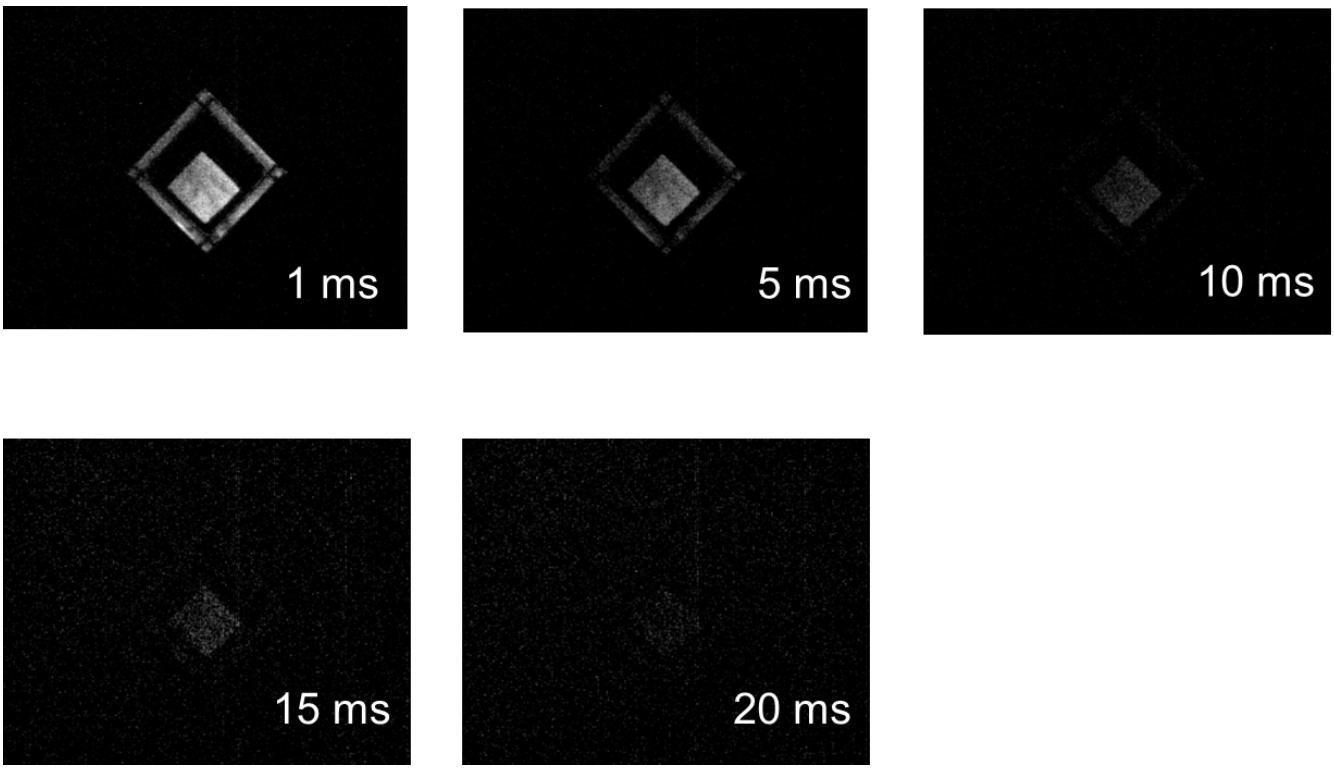

Figure S14. Time-delayed luminescence imaging of the two-square pattern encoded with $NaYF_4$: 20% Yb^{3+}, 40% Er^{3+}@ $NaYbF_4$@ $NaYF_4$@ $NaYF_4$: 20% Nd^{3+}core/multi-shell nanoparticles of two distinct lifetimes (6.37 and 4.03 ms), which was immersed in intralipid solution at a 6 mm depth.